Dalton Transactions

ROYAL SOCIETY OF CHEMISTRY

PAPER

View Article Online
View Journal | View Issue

Cite this: *Dalton Trans.*, 2023, **52**, 11503

β-(*Z*)-Selective alkyne hydrosilylation by a N,O-functionalized NHC-based rhodium(I) catalyst†

Miguel González-Lainez, M. Victoria Jiménez, * Vincenzo Passarelli and Jesús J. Pérez-Torrente *

Neutral and cationic cyclooctadiene rhodium(I) complexes with a lutidine-derived polydentate ligand having NHC and methoxy side-donor functions, [RhBr(cod)(κC-^{t}BuImCH$_2$PyCH$_2$OMe)] and [Rh(cod)(κ^{2}C,N-^{t}BuImCH$_2$PyCH$_2$OMe)]PF$_6$, have been prepared. Carbonylation of the cationic compound yields the dicarbonyl complex [Rh(CO)$_2$(κ^{2}C,N-^{t}BuImCH$_2$PyCH$_2$OMe)]PF$_6$ whereas carbonylation of the neutral compound affords a mixture of di- and monocarbonyl neutral complexes [RhBr(CO)$_2$(κC-^{t}BuImCH$_2$PyCH$_2$OMe)] and [RhBr(CO)(κ^{2}C,N-^{t}BuImCH$_2$PyCH$_2$OMe)]. These complexes efficiently catalyze the hydrosilylation of 1-hexyne with HSiMe$_2$Ph with a marked selectivity towards the β-(*Z*)-vinylsilane product. Catalyst [RhBr(CO)(κ^{2}C,N-^{t}BuImCH$_2$PyCH$_2$OMe)] showed a superior catalytic performance, in terms of both activity and selectivity, and has been applied to the hydrosilylation of a range of 1-alkynes and phenylacetylene derivatives with diverse hydrosilanes, including HSiMe$_2$Ph, HSiMePh$_2$, HSiPh$_3$ and HSiEt$_3$, showing excellent β-(*Z*) selectivity for the hydrosilylation of linear aliphatic 1-alkynes. Hydrosilylation of internal alkynes, such as diphenylacetylene and 1-phenyl-1-propyne, selectively affords the *syn*-addition vinylsilane products. The β-(*Z*) selectivity of these catalysts contrasts with that of related rhodium(I) catalysts based on 2-picolyl-functionalised NHC ligands, which were reported to be β-(*E*) selective. An energy barrier $\Delta G^{\ddagger}$ of 19.8 ± 2.0 kcal mol^{-1} (298 K) has been determined from kinetic studies on the hydrosilylation of 1-hexyne with HSiMe$_2$Ph. DFT studies suggest that the methoxy-methyl group is unlikely to be involved in the activation of hydrosilane, and then hydrosilane activation is likely to proceed *via* a classical Si–H oxidative addition.

Received 20th June 2023,
Accepted 27th July 2023

DOI: 10.1039/d3dt01911j

rsc.li/dalton

Introduction

Unsaturated silyl derivatives are valuable synthetic intermediates due to their versatility, ease of handling, low toxicity and stability, as well as their compatibility with many organic transformations.[1] In particular, vinylsilanes have applications as crosslinking agents in the silicone industry and, in general, in the polymer industry.[2] In this regard, the hydrosilylation of terminal alkynes is the most direct, powerful and atom-economical route for the preparation of vinylsilanes.[3] Since the first example of metal-catalyzed hydrosilylation of terminal alkynes described by Sommer *et al.* in the mid-1940s,[4] this has been the preferred method for the production of vinylsilanes to date. A large number of catalysts based on both noble metals and more abundant, cheaper and harmless metals, have been developed.[5] However, in spite of their great projection at the industrial level, most metal catalysts present the disadvantages derived from the formation of isomers, which implies lower selectivity and yield, and consequently, lower quality of the final products.

The hydrosilylation of terminal alkynes can give rise to three possible vinylsilane isomers: the isomers β-(*Z*) and β-(*E*) derived from anti-Markovnikov addition, *trans* and *syn* addition, respectively, and the isomer α derived from Markovnikov addition (Scheme 1). In addition, in some cases, the dehydrogenative silylation products, the silyl-alkyne deriva-

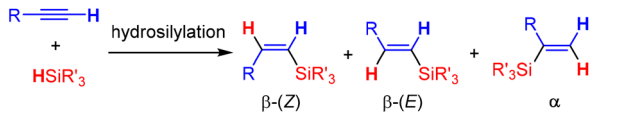

Scheme 1 Possible vinylsilane products in the hydrosilylation of terminal alkynes.

Departamento de Química Inorgánica, Instituto de Síntesis Química y Catálisis Homogénea-ISQCH, Universidad de Zaragoza-C.S.I.C., 50009-Zaragoza, Spain. E-mail: vjimenez@unizar.es

† Electronic supplementary information (ESI) available: ^{1}H, ^{13}C NMR and ATR-IR spectra for the organometallic compounds. Hammett plot, additional experimental catalytic data and kinetic studies. Coordinates of calculated structures (*XYZ*). CCDC 2248980 (**6**), 2248981 (**3**) and 2248982 (**2**). For ESI and crystallographic data in CIF or other electronic format see DOI: **https://doi.org/10.1039/d3dt01911j**

tive and the alkene resulting from the reduction of the alkyne, are obtained as by-products.[6] In general, the selectivity depends on several factors including the catalyst, the substituents on the hydrosilane and alkyne, and the reaction conditions. Therefore, the design of new ligands to modulate the electronic and steric properties of the metal centre is key to achieve selective and efficient catalysts for the large-scale application of this methodology.

Transition-metal complexes containing N-heterocyclic carbenes (NHCs) have been powerful tools in catalysis for the past 20 years,[7] with a wide range of applications illustrating the versatility of this type of compounds. In this regard, there has been significant interest in the design of NHC-based alkyne hydrosilylation catalysts that include noble[8] and, more recently, non-noble transition metals[9] with the aim of developing active catalysts to control both regioselectivity and stereoselectivity. Despite the high price, the high activity and stability of rhodium, iridium and platinum based catalysts have stimulated research in this field. In this context, it is worth mentioning the excellent performance of NHC–Pt(0) catalysts developed by Markó, that preferentially afford the β-(*E*)-vinylsilane isomer in the hydrosilylation of terminal alkynes.[10] Interestingly, a selectivity model based on structural parameters of the NHC ligand has been devised to rationalize the regioselectivity.[10,11] In contrast, NHC–Rh(I) and Ir(I) catalysts have shown high activities but with variable selectivity, in some cases due to their ability to perform the isomerization of the less thermodynamically stable β-(*Z*) isomer into the β-(*E*)-vinylsilane isomer.[6,12] A preference for the β-(*Z*)-vinylsilane isomer was found for coumarin-[13] and alkenyl-functionalized[14] NHC–Ir(I) catalysts. Similarly, rhodium(I) catalysts based on triazolylidene ligands exhibited good selectivity for the β-(*Z*) vinylsilane isomer with the related cyclometalated Cp*–Rh(III) catalysts being even much more active and selective.[15] However, β-(*E*) selectivity was observed in the hydrosilylation of aromatic alkynes with a 3-(trimethoxysilyl)propyl-functionalized NHC–Rh(I) catalyst, whereas related NHC–Cp*Rh(III) catalysts showed excellent β-(*Z*) selectivity. Interestingly, a selectivity shift towards β-(*Z*) was observed after immobilization of the NHC–Rh(I) catalyst on mesoporous SBA-15.[16]

Rhodium(I) complexes bearing N-functionalized NHC ligands have received considerable attention as hydrosilylation catalysts (Fig. 1). Our research group described amino-alkyl-functionalized NHC–Rh(I) catalysts that proved to be β-(*Z*) selective in 1-hexyne hydrosilylation but β-(*E*) selective in the hydrosilylation of sterically hindered alkynes. In addition, β-(*Z*) → β-(*E*) vinylsilane isomerization was observed at prolonged reaction times, along with extensive polymerization of phenylacetylene.[17] Cassani and Mazzoni also observed β-(*Z*) → β-(*E*) isomerization for neutral Rh(I) complexes containing a BOC-protected amino-alkyl-functionalized NHC ligand, but phenylacetylene polymerization was not observed. Although a slight increase in activity was observed due to the presence of the bulky hemilabile group, steric hindrance on the substituent in the NHC ligand or alkyne substrates affected conversion and selectivity very negatively.[18] The catalytic activity of 2-picolyl-functionalized NHC–Rh(I) catalyst in alkyne hydrosilylation was studied by Peris[12] and, recently, by Salazar and Suárez.[19] Peris' catalyst afforded a mixture of β-(*Z*)/β-(*E*) vinylsilane isomers in the hydrosilylation of phenylacetylene with $HSiMe_2Ph$ at high temperature (60 °C), although β-(*Z*) selectivity was improved at room temperature.[12] Salazar and Suarez reported a series of cationic picolyl-functionalized NHC–Rh(I) catalyst precursors having different substituent at the 6-position of the pyridine donor. These compounds efficiently catalyzed the hydrosilylation of terminal alkynes with excellent β-(*E*) selectivity. The increase of the steric hindrance in the picolyl fragment resulted in a very efficient catalyst with improved selectivity for the β-(*E*)-vinylsilane isomer in the hydrosilylation of a variety of alkynes with both electron-rich and electron-poor hydrosilanes.[19] Aiming at studying the effect of ligand rigidity, Bera and co-workers have recently reported a Rh(I) complex with a NHC ligand based on fused π-conjugated imidazo[1,5-*a*]naphthyridine bearing a bulky diisopropylphenyl substituent on the imidazole ring (Fig. 1). This compound has been shown to be an excellent catalyst precursor for accessing β-(*E*)-vinylsilanes in the hydrosilylation of a range of terminal alkynes with the hydrosilanes Et_3SiH and $(EtO)_3SiH$.[20]

Inspired by these results, we envisaged the potential of Rh(I) complexes based on a lutidine-derived polydentate ligand having NHC and methoxy side-donor functions as hydrosilylation catalysts. The incorporation of a flexible methoxy-methyl functionality, $-CH_2OMe$, at the 6-position of the pyridine donor moiety, in close proximity to the rhodium centre, might have an impact on the outcome of the hydrosilylation reactions. The potential hemilabile character of this donor function could enable the stabilization of coordinately unsaturated or polar catalytic intermediates, or the promotion of directing effects with substrates.[21] In this connection, it is worth noting

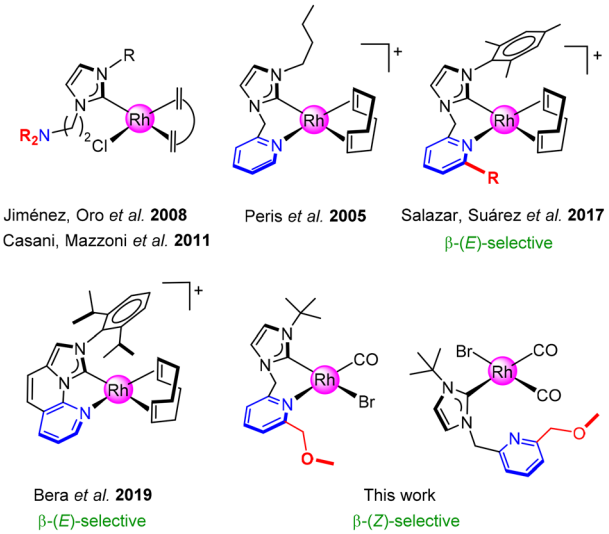

Fig. 1 Rhodium(I) catalysts based on 2-pyridylmethyl-functionalized N-heterocyclic carbene ligands for the hydrosilylation of terminal alkynes.

that improved catalytic performance in transfer hydrogenation and hydrogen autotransfer reactions has been observed for iridium catalysts based on methoxy-functionalized NHC ligands.[22] Herein we report on the synthesis of neutral and cationic rhodium(I) diene and carbonyl complexes based on this N,O-functionalized NHC ligand (Fig. 1) and their remarkable β-(*Z*) selectivity in catalyzed hydrosilylation of terminal alkynes under mild conditions.

Results and discussion

Synthesis and structure of rhodium(I) diene complexes with an N,O-functionalized NHC ligand

The direct deprotonation of the methoxy-functionalized lutidine-derived imidazolium salt [^{t}BuHImCH$_2$PyCH$_2$OMe]Br (**1**) by the bridging methoxo ligands of the dinuclear complex [Rh(μ-OMe)(cod)]$_2$ gave the square planar neutral bromo complex [RhBr(cod)(κC-^{t}BuImCH$_2$PyCH$_2$OMe)] (**2**) which was isolated as a yellow solid in 96% yield (Scheme 2). Compound **2** is soluble in both polar and non-polar solvents and, in agreement with its neutral character, is non-conductor in acetone. The formation of the Rh–NHC bond was confirmed by the presence of a low-field doublet resonance at δ 182.3 ppm (J_{Rh-C} = 50.1 Hz) in the $^{13}C\{^1H\}$ NMR spectrum which was assigned to the C2 carbene carbon atom of the imidazole ring (N*C*N).[17] The =CH protons and carbons of the cod ligand showed four resonances in the spectra, which is in accordance with the axial chirality arising from restricted rotation around the Rh–NHC bond. The =CH *trans* to the NHC moiety were observed more unshielded both in the ^1H and $^{13}C\{^1H\}$ NMR spectra, with smaller J_{Rh-C} coupling constants, compared to the =CH *trans* to bromido.[13,23] The diastereotopic protons of the methylene linker Im–CH$_2$–Py were observed as two well-separated doublets at δ 6.91 and 5.99 ppm (J_{H-H} = 14.7 Hz). However, the methylene protons of Py–CH$_2$–OMe showed an AB system with very close chemical shifts, which is attributed to the conformational freedom of this uncoordinated fragment.[24]

Reaction of **2** with one equivalent of AgPF$_6$ in dichloromethane resulted in the precipitation of AgBr and the formation of a yellow solution of the cationic complex [Rh(cod)(κ^{2}C,N-^{t}BuImCH$_2$PyCH$_2$OMe)]PF$_6$ (**3**), which was isolated as a yellow microcrystalline solid in 96% yield (Scheme 2). The abstraction of the bromido ligand allows the generation of a coordination vacancy which is occupied by the pyridine fragment of the functionalized NHC ligand thus adopting a κ^{2}C,N coordination (see below). The high-resolution ESI$^+$ mass spectrum, that shows the molecular ion at 470.1673 *m*/*z*, and the conductivity of 78 Ω^{-1} cm^2 mol^{-1} measured in nitromethane, a typical value for 1 : 1 electrolytes, support the cationic formulation of **2**. The coordination of the pyridine fragment in **3** is evidenced in the ^1H NMR spectrum by the high field shift of the resonances ascribed to the diastereotopic protons of the methylene linker Im–CH$_2$–Py.

The molecular structure of compounds [RhBr(cod)(κC-^{t}BuImCH$_2$PyCH$_2$OMe)] (**2**) and [Rh(cod)(κ^{2}C,N-^{t}BuImCH$_2$PyCH$_2$OMe)]PF$_6$ (**3**) were determined by an X-ray diffraction analysis. The molecular structure of **2** (Fig. 2 – top) shows a distorted square planar geometry of the metal centre with a *cis* arrangement of the NHC and bromido ligands [C1–Rh1–Br1 86.48(6)°, Rh1–C1 2.042(2) Å, Rh1–Br1 2.5156(3) Å] and with the cod ligand occupying the two remaining *cis* positions [ct1–Rh1–ct2 87.387(10)°]. Reasonably as a consequence of the higher *trans* influence of the NHC ligand when compared to the bromido ligand, the Rh1–ct1 distance [2.0783(2) Å] is longer than the Rh1–ct2 distance [1.9924(2) Å]. Accordingly, the C20–C21 bond length [1.376(4) Å] is shorter than the C24–C25 bond length [1.410(3) Å] confirming a higher degree of π-backdonation to the olefin bond C24–C25 when compared with C20–C21. The NHC ring lies almost perpendicular to the coordination plane [N2–C1–Rh1–Br1 −93.24(21)°], which corresponds to the least hindered disposition, and exhibits a slightly distorted arrangement with respect to the Rh1–C1 bond (pitch, θ 2.3°; yaw, ψ 4.7°).

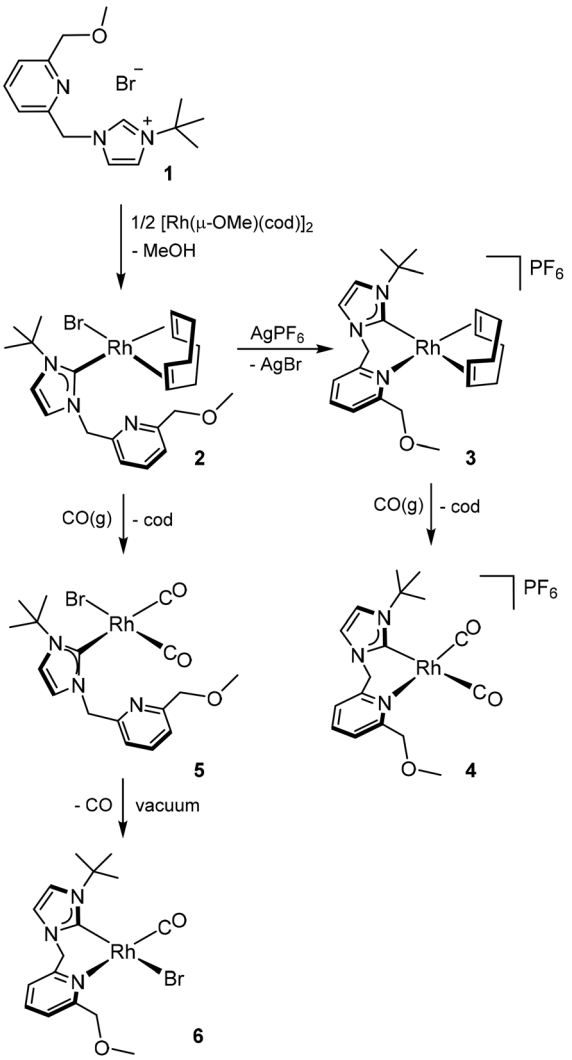

Scheme 2 Synthetic pathway for the preparation of rhodium(I) complexes bearing a lutidine-based NHC/OMe functionalized ligand.

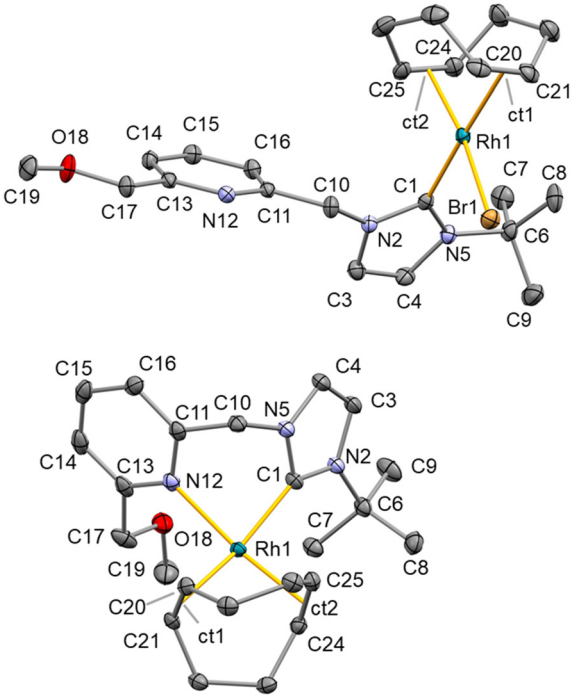

Fig. 2 ORTEP view of **2** (top) and **3** (bottom). Thermal ellipsoids are at 50% probability. For the sake of clarity, hydrogen atoms are omitted and only the cation is shown for **3**. Selected bond lengths (Å) and angles (°) are: **2**, C1–Rh1 2.042(2), Br1–Rh1 2.5156(3), ct1–Rh1 2.0783(2), ct2–Rh1 1.9924 (2), C20–C21 1.376(4), C24–C25 1.410(3), C1–Rh1–Br1 86.48(6), C1–Rh1–ct1 178.09(6), ct2–Rh1–ct1 87.387(10), ct2–Rh1–C1 93.74(6), ct2–Rh1–Br1 169.639(10), ct1–Rh1–Br1 92.682(11); **3**, C1–Rh1 2.0618(19), N12–Rh1 2.1331(17), Rh1–ct2 2.0215(2), Rh1–ct1 2.0989(2), C20–C21 1.366(3), C24–C25 1.379(3), C1–Rh1–N12 81.23(7), C1–Rh1–ct1 163.20(5), ct2–Rh1–C1 95.52(5), ct1–Rh1–N12 93.37(4), ct2–Rh1–N12 168.02(5), ct2–Rh1–ct1 86.488(10). ct1 and ct2 are the centroids of the olefinic bonds.

Fig. 2 – bottom shows the molecular structure of **3**. A distorted square planar coordination of the metal centre is observed with the cod ligand occupying two mutually *cis* positions [ct2–Rh1–ct1 86.488(10)°] and the κ^2C,N coordinated ligand at the remaining coordination sites [C1–Rh1 2.0618(19) Å, N12–Rh1 2.1331(17) Å, C1–Rh1–N12 81.23(7)°]. The bidentate coordination of the functionalized NHC ligand renders the six-member metalacycle Rh1–C1–N5–C10–C11–N12 exhibiting a boat conformation with the atoms Rh1 and C10 occupying the out-of-plane positions.

Notably, as a consequence of the bidentate coordination of the functionalized NHC ligand, the NHC moiety tilts away from the almost perpendicular arrangement with respect to the coordination plan [N5–C1–Rh1–N12 54.43(14)°]. By the same token, the pyridine core also deviates from the least hindered perpendicular arrangement with respect to the coordination plane [C11–N12–Rh1–C1 −59.87(15)°]. Also, the NHC moiety significantly deviates from the ideal arrangement with respect to the bond Rh1–C1 (pitch, θ 3.1°; yaw, ψ 15.6°) whereas a smaller deviation of the pyridine core is observed with respect to the bond Rh1–N12 (pitch, θ 6.8°; yaw, ψ 5.6°). Finally, it is worth a mention that similar Rh1–ct1 [2.0989(2) Å] and Rh1–ct2 distances [2.0215(2) Å] along with similar C20–C21 [1.366(3) Å] and C24–C25 bond lengths [1.379(3) Å] suggest that the *trans* influence of the pyridine and NHC moieties are similar in **3**.

Carbonylation of rhodium(I) diene complexes 2 and 3

The 1,5-cyclooctadiene ligand in complexes [RhBr(cod)(κC-^{t}BuImCH$_2$PyCH$_2$OMe)] (**2**) and [Rh(cod)(κ^2C,N-^{t}BuImCH$_2$PyCH$_2$OMe)]PF$_6$ (**3**) is readily displaced by carbon monoxide. Bubbling of carbon monoxide through a dichloromethane solution of the cationic complex **3** for 5 min at room temperature afforded a pale yellow solution from which compound [Rh(CO)$_2$(κ^2C,N-^{t}BuImCH$_2$PyCH$_2$OMe)]PF$_6$ (**4**) was isolated as a yellow solid in 78% yield (Scheme 2). The ATR-IR spectrum of **4** showed two strong ν(CO) stretching bands at 2081 and 2008 cm^{-1} which agrees with the presence of two carbonyl ligands in *cis*-arrangement.[24,25] The low-field region of the ^{13}C{^{1}H} NMR spectrum showed three doublets, two of them at δ 185.5 (J_{Rh-C} = 74.0 Hz, CO$_{trans\text{-Py}}$) and 184.6 ppm (J_{Rh-C} = 55.9 Hz, CO$_{trans\text{-NHC}}$) correspond to the carbonyl ligands, and the third one at δ 168.9 ppm (J_{Rh-C} = 43.7 Hz) is assigned to the N*C*N carbenic carbon atom. In agreement with the unsymmetrical structure of **4**, resulting from the κ^2C,N coordination of the ligand, the protons of both methylene linkers are diastereotopic and, consequently, were observed as two AB systems centered at δ 5.75 (Im–CH$_2$–Py) and 4.67 (Py–CH$_2$–OMe) ppm.[13]

Carbonylation of the neutral compound [RhBr(cod)(κC-^{t}BuImCH$_2$PyCH$_2$OMe)] (**2**) in dichloromethane for 5 min at room temperature also gave a pale-yellow solution. However, standard work up resulted in a mixture of complexes [RhBr(CO)$_2$(κC-^{t}BuImCH$_2$PyCH$_2$OMe)] (**5**) and [RhBr(CO)(κ^2C,N-^{t}BuImCH$_2$PyCH$_2$OMe)] (**6**). The neutral *cis*-dicarbonyl complex **5** is the expected compound resulting from the substitution of the cod ligand by two carbonyl ligands. However, the formation of **6** is a consequence of the elimination of a CO ligand in **5** under vacuum, and the coordination of the pyridine fragment of the ligand (Scheme 2). Compounds **5** and **6** were prepared independently using different synthetic strategies. Bubbling CO(g) through a solution of **2** in dichloromethane until complete evaporation of the solvent gave **5**, which was isolated under a carbon monoxide atmosphere as a yellow solid in 94% yield. On the other hand, if after bubbling CO(g) for 5 min the solution is evaporated to dryness under vacuum, compound **6** can be extracted from the resulting oily residue by successive washing with diethyl ether and isolated as a yellow solid in 49% yield. Accordingly, the solid residue obtained after extraction of **6** was identified as compound **5**.

The ATR-IR spectrum of **5** showed two strong ν(CO) stretching bands at 2066 and 1988 cm^{-1}, with a $\Delta\nu_{CO}$ of 78 cm^{-1} in agreement with a *cis* di-carbonyl compound, while a single strong band at 1963 cm^{-1} was observed in the spectrum of **6**. The ^{13}C{^{1}H} NMR spectrum of **5** showed two doublet resonances at δ 186.1 (J_{Rh-C} = 54.1 Hz) and 182.4 (J_{Rh-C} = 77.8 Hz) ppm assigned to the carbonyl ligands *trans* to NHC and Br, respectively.[13] As expected, a single resonance at δ 191.2 ppm

(J_{Rh-C} = 34.6 Hz) was observed for **6**. The ^{1}H NMR spectrum of **5** evidenced that, despite the presence of much less bulky carbonyl ligands, the rotation around the Rh–C bond is restricted. The methylene linker Im–CH_2–Py were observed as an AB system in **5** and two doublets in **6**. However, the methylene protons of Py–CH_2–OMe were observed as a singlet in **5** and as two doublets in **6** which agree with the conformational freedom of the uncoordinated Py–CH_2–OMe fragment in **5** and the conformational restriction imposed by the coordination of the pyridine moiety in **6** (see Fig. S22 of the ESI†).

The molecular structure of [RhBr(CO)(κ^{2}C,N-^{t}BuImCH$_2$PyCH$_2$OMe)] (**6**), determined by means of an X-ray diffraction study on a single crystal of **6**, confirms the formation of the SP-4-4 isomer having the carbonyl ligand *trans* to pyridine (Fig. 3). A distorted square planar geometry is observed at the metal centre in **6**. The κ^{2}C,N coordinated ligand occupies two mutually *cis* position [C1–Rh1 1.988(3) Å, N12–Rh1 2.165(3) Å, C1–Rh1–N12 83.17(11)°] and the bromido and carbonyl ligands lie at the remaining *cis* coordination sites [N12–Rh1 2.165(3) Å, Br1–Rh1 2.5162(4) Å, C20–Rh1–Br1 89.94(10)°], with the bromido ligand *trans* to the carbenic carbon atom C1 [C1–Rh1–Br1 176.31(9)°]. Similar to **3**, a boat conformation of the six-member cycle Rh1–C1–N5–C10–C11–N12 is observed in **6** with the atoms Rh1 and C10 at the out-of-plane positions. Also, both the NHC and pyridine cores deviate from the least hindered disposition perpendicular to the coordination plane [C1–N12–Rh1–C1 −57.97(24)°; N5–C1–Rh1–N12 47.53(24)°]. Nonetheless, it is worth a mention that when comparing **6** with **3**, even if similar pitch and yaw angles are observed for the NHC moieties (**3**: pitch, θ 3.1°; yaw, ψ 15.6°; **6**: pitch, θ 3.5°; yaw, ψ 11.1°), and the pyridine cores feature similar yaw angles (**3**: yaw, ψ 5.6°; **6**: yaw, ψ 5.2°), substantially different pitch angles are observed for the pyridine moieties (**3**: pitch, θ 6.8°; **6**: pitch, θ 12.5°) reasonably suggesting that a subtle electronic influence of the ancillary ligands is exerted on the coordination of the pyridine moiety. Interestingly, related halo-carbonyl complexes featuring κ^{2}C,N bidentate oxazolinyl- and benzoxazole-functionalized NHC ligands also exhibited the halogenido ligand *trans* to the NHC moiety.[26]

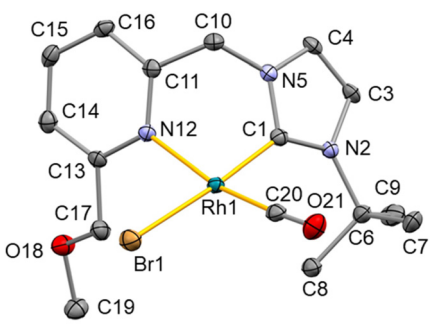

Fig. 3 ORTEP view of **6**. Thermal ellipsoids are at 50% probability and hydrogen atoms are omitted for clarity. Selected bond lengths (Å) and angles (°) are: C1–Rh1 1.988(3), N12–Rh1 2.165(3), Br1–Rh1 2.5162(4), C20–Rh1 1.814(3), C20–O21 1.140(4), C1–Rh1–N12 83.17(11), C20–Rh1–N12 168.08(12), C1–Rh1–Br1 176.31(9), C20–Rh1–Br1 89.94(10).

Hydrosilylation of 1-hexyne catalyzed by rhodium(I) complexes: catalyst screening

The potential of the rhodium(I) compounds based on the N,O-functionalized NHC ligand shown in Scheme 2 as hydrosilylation catalysts has been investigated using the hydrosilylation of 1-hexyne with $HSiMe_2Ph$ as the model reaction. The catalytic reactions were performed under an argon atmosphere in $CDCl_3$ (0.5 mL) at 333 K with 1 mol% catalyst loading, [catalyst] = 2.2 mM, and routinely monitored by ^{1}H NMR until practically quantitative conversions. The outcome of these preliminary experiments is summarized in Table 1.

Rhodium compounds **2–6** were found to be selective to the β-(*Z*)-vinylsilane isomer (62–90%). The neutral complexes were more selective for the β-(*Z*)-vinylsilane isomer than the cationic counterparts. For instance, compound [RhBr(cod)(κC-^{t}BuImCH$_2$PyCH$_2$OMe)] (**2**) yielded 79% of the β-(*Z*)-vinylsilane isomer (entry 2) whereas 57% of this isomer was obtained with the cationic analogue [Rh(cod)(κ^{2}C,N-^{t}BuImCH$_2$PyCH$_2$OMe)]PF$_6$ (**3**) (entry 3). The same trend was observed when comparing the cationic [Rh(CO)$_2$(κ^{2}C,N-^{t}BuImCH$_2$PyCH$_2$OMe)]PF$_6$ (**4**) and the neutral [RhBr(CO)$_2$(κC-^{t}BuImCH$_2$PyCH$_2$OMe)] (**5**) carbonyl complexes, which afforded selectivities of 62% and 89% to the β-(*Z*)-vinylsilane isomer, respectively (entries 4 and 5). When comparing the selectivity for the β-(*Z*)-vinylsilane isomer achieved with related diene and carbonyl compounds, the neutral carbonyl complex **5** was more selective than the diene complex **2**, 89 *vs.* 79%, respectively (entries 2 and 5). However, similar selectivities of around 60% were attained with both the cationic diene **2** and carbonyl complexes **3** and **4** (entries 3 and 4). From the activity point of view, the neutral diene complex **2** and the cationic carbonyl complex **4** proved to be the most active, with complete conversion in 35 min (entries 2 and 4). To our delight, the unusual complex [RhBr(CO)(κ^{2}C,N-^{t}BuImCH$_2$PyCH$_2$OMe)] (**6**) showed the best catalytic performance, both in terms of activity and selectivity, providing complete conversion with 90% selectivity for the β-(*Z*)-vinylsilane isomer in 30 min (entry 6). Finally, for the sake of comparison, the diene iridium(I) compound, [IrBr(cod)(κC-^{t}BuImCH$_2$PyCH$_2$OMe)] (**7**),[24] was found to be much less active than the related rhodium complex **2**, affording the β-(*Z*)-vinylsilane product with moderate selectivity (entry 7). The catalytic performance of **6** was evaluated at 0.1 mol% catalyst loading, giving 99% conversion after 8 h with a 85% selectivity for the β-(*Z*)-vinylsilane product.

It is worth noting that the β-(*Z*) selectivity observed in the hydrosilylation of 1-hexyne with $HSiMe_2Ph$ with rhodium(I) catalysts **2–6** contrasts with that observed by Salazar and Bera with related cationic diene compounds based on NHC–Py[19] or NHC–naphthyridine[20] bidentate ligands with very bulky substituents on the NHC fragment, as both showed excellent β-(*E*) selectivities in the hydrosilylation of a number of terminal alkynes.

Table 1 Hydrosilylation of 1-hexyne with $HSiMe_2Ph$ catalyzed by Rh(I)–NHC–Py–OMe compounds[a]

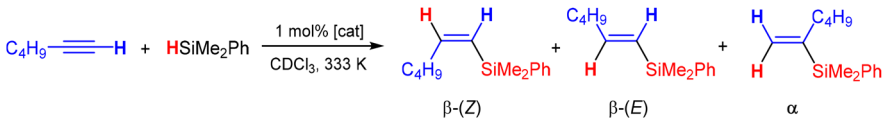

	Catalyst		Time	Conversion[b] (%)	Selectivity[b] (%)		
					β-(*Z*)	β-(*E*)	α
1	No catalyst		3 h	0	—	—	—
2	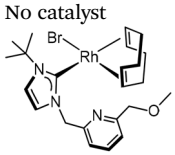	**2**	35 min	100	79	16	5
3	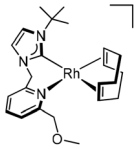	**3**	2 h	98	57	33	10
4	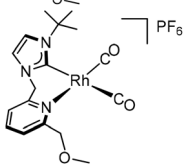	**4**	30 min	97	62	29	9
5	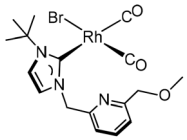	**5**	75 min	100	89	7	4
6	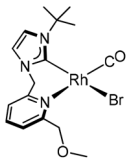	**6**	30 min	100	90	6	4
7	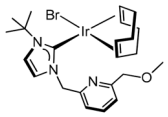	**7**	70 h	100	65	22	12

[a] Reaction conditions: 1-hexyne (0.11 mmol), $HSiMe_2Ph$ (0.11 mmol) and catalyst (0.0011 mmol, 1.0 mol%), in $CDCl_3$ (0.5 mL) at 333 K. $[HSiMe_2Ph] = [1\text{-hexyne}] \approx 0.22$ M. [b] Conversion, based on $HSiMe_2Ph$, and selectivity determined by ^1H NMR using anisole as internal standard.

Hydrosilylation of alkynes catalyzed by $[Rh(CO)_2(\kappa^2C, N\text{-}^t\text{BuImCH}_2\text{PyCH}_2\text{OMe})]PF_6$ (6): substrate scope

The catalytic performance of compound **6** prompted us to explore the substrate scope in the hydrosilylation of 1-alkynes using different hydrosilanes under the reaction conditions described before (Table 2).

The hydrosilylation of linear aliphatic 1-alkynes, such as 1-hexyne and 1-octyne, was completed in 30 and 20 min, respectively, with selectivities to β-(*Z*)-vinylsilane around 90% (entries 1 and 2). In contrast, the hydrosilylation of a branched aliphatic alkyne, such as the bulky 3,3-dimethyl-1-butyne, was much slower, reaching 92% conversion in 6 h to give a mixture of β-(*E*)- and α-vinylsilane products (entries 3 and 4). Similarly, hydrosilylation of ester-functionalized alkynes, such as methyl propiolate, was unselective and gave the β-(*Z*)- and α-vinylsilane products, 44 and 47%, respectively, along with 13% methyl acrylate, the hydrogenation product, after 3 h (entry 5).

The hydrosilylation of phenylacetylene with $HSiMe_2Ph$ was completed in 3 h and provided a 67% β-(*Z*) selectivity (entry 6). Interestingly, the formation of polyphenylacetylene was not observed. In sharp contrast, the neutral diene catalyst [RhBr(cod)(κ-*C*-^{t}BuImCH$_2$PyCH$_2$OMe)] (**2**) quantitatively polymerized phenylacetylene in 30 min under the same reaction conditions, in agreement with what was observed with previously reported Rh(I)–diolefin catalysts.[27] The influence of electronic effects on the hydrosilylation of terminal alkynes was studied in a series of phenylacetylene derivatives with different substituents at the *para* position. The hydrosilylation of 4-ethynylani-

Table 2 Hydrosilylation of terminal alkynes with $HSiMe_2Ph$ catalyzed by [RhBr(CO)(κ^2C,N-^{t}BuImCH$_2$PyCH$_2$OMe)] (**6**)[a]

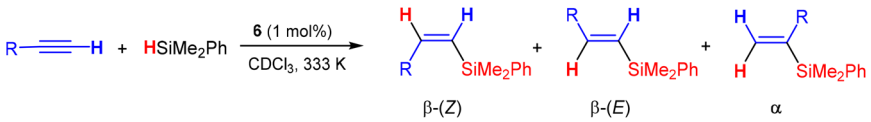

β-(*Z*) β-(*E*) α

	Silane	Alkyne	Time	Conversion[b] (%)	Selectivity[b] (%)		
					β-(*Z*)	β-(*E*)	α
1	$HSiMe_2Ph$	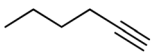	30 min	100	90	6	4
2	$HSiMe_2Ph$	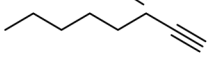	20 min	100	88	6	6
3	$HSiMe_2Ph$	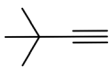	30 min	28	2	67	31
4			6 h	92	5	55	40
5[c]	$HSiMe_2Ph$	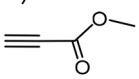	3 h	100	—	44	47
6	$HSiMe_2Ph$	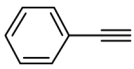	3 h	100	67	21	12
7	$HSiMe_2Ph$	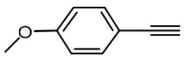	1 h 15 min	91	68	24	8
8[d]	$HSiMe_2Ph$	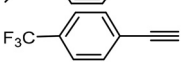	5 h	95	57	26	17
9	$HSiMe_2Ph$	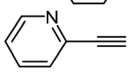	24 h	23	43	49	8
10	$HSiMe_2Ph$	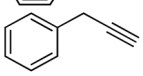	6 h	96	77	15	8
11	$HSiMePh_2$	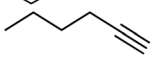	30 min	95	100	—	—
12	$HSiPh_3$	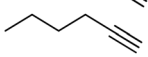	24 h	87	100	—	—
13	$HSiEt_3$	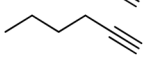	1 h 30 min	97	89	6	5
14	$HSiMe_2Et$	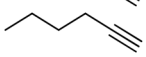	30 min	98	89	7	4
15	$HSiMePh_2$	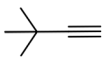	24 h	100	8	40	52
16	$HSiMePh_2$	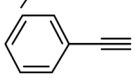	24 h	59	29	43	28
17	$HSiMePh_2$	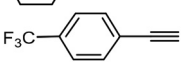	24 h	59	22	51	27
18	$HSiMePh_2$	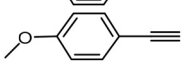	24 h	100	42	39	19

[a] Reaction conditions: alkyne (0.11 mmol), $HSiR_3$ (0.11 mmol) and **6** (0.0011 mmol, 1.0 mol%), in $CDCl_3$ (0.5 mL) at 333 K. [$HSiR_3$] = [1-alkyne] ≈ 0.22 M. [b] Conversion, based on $HSiR_3$, and selectivity determined by ^{1}H NMR using anisole as internal standard. [c] 9% of methyl acrylate. [d] Traces of 1-trifluoromethyl-4-vinylbenzene were observed.

sole is faster than that of phenylacetylene, reaching 91% of conversion in 75 min with similar selectivity (entry 7). However, the hydrosilylation of 1-ethynyl-4-(trifluoromethyl) benzene was slower, requiring 5 h to reach 95% conversion, with a decrease of β-(*Z*) selectivity to 57% (entry 8). The difference of activity observed for the hydrosilylation of 4-R–C_6H_4–C≡CH derivatives (R = H, MeO and CF_3) with $HSiMe_2Ph$ is in agreement with the negative slope of the Hammett plot (ρ = −0.37 for TOF_{50}; see ESI†). As a matter of fact, the activity slightly increases with the alkyne with an electron-donating group and decreases when an electron-withdrawing substituent is present, taking phenylacetylene as the benchmark. Thus, it can be argued that a positive charge accumulation is occurring in the transition state and, consequently, a rate increase by electron donating groups is observed due to resonance stabilization. It should be noted that a similar behavior has also been observed for related triazolylidene-based rhodium and iridium catalysts.[15b,28]

The hydrosilylation of 2-ethynylpyridine, an alkyne functionalized with a π-electron-deficient heterocycle, had a poor outcome as only 23% conversion was achieved in 24 h (entry 9), probably due to the coordinative ability of the pyridine frag-

ment which competes with the triple bond. Finally, the benzyl alkyne 3-phenyl-1-propyne was much more reactive reaching a 96% conversion in 7 h with 77% selectivity to the β-(*Z*)-vinylsilane isomer (entry 10).

The influence of the hydrosilane on the **6**-catalyzed hydrosilylation of 1-hexyne has also been studied. For this purpose, hydrosilanes with different steric hindrance such as $HSiMePh_2$, $HSiPh_3$, $HSiEt_3$ and $HSiMe_2Et$ have been used (Table 2, entries 11–14). The hydrosilylation of 1-hexyne with $HSiMePh_2$ and $HSiPh_3$ selectively produced the β-(*Z*)-vinylsilane isomer. However, the catalytic activity is largely influenced by the steric demand of the hydrosilane. Thus, 95% conversion was achieved with $HSiMePh_2$ in only 30 min, although in the case of the bulkier $HSiPh_3$ it took 24 h to reach 87% of conversion (entries 11 and 12). On the other hand, less bulky hydrosilanes, such as $HSiEt_3$ and $HSiMe_2Et$, were much more reactive affording conversions higher than 95% in 1.5 and 0.5 h, respectively, with 89% selectivity for the β-(*Z*)-vinylsilane isomer (entries 13 and 14). The excellent catalytic performance of catalyst **6** in the hydrosilylation of 1-hexyne with $HSiMePh_2$ prompted us to study its reactivity with other terminal alkynes. Hydrosilylation of 3,3-dimethyl-1-butyne with $HSiMePh_2$ proceeded slowly, with complete conversion in 24 h, to give a mixture of isomers in which α-vinylsilane (52%) was the major product (entry 15). Unfortunately, also the hydrosilylation of aromatic alkynes with $HSiMePh_2$ was not selective regardless of the electronic character of the *para* substituent, although the same reactivity trend as found for $HSiMe_2Ph$ was observed (entries 16–18).

Finally, **6** is a good catalyst for the hydrosilylation of symmetric (diphenylacetylene) and asymmetric (1-phenyl-1-propyne) internal alkynes under the same conditions (Table 3, entries 1–4). The hydrosilylation of diphenylacetylene with $HSiMe_2Ph$ was completely selective to the *syn* addition product, *E* isomer, reaching 94% conversion in 2 h (entry 2). However, the hydrosilylation of 1-phenyl-1-propyne was slower, 95% conversion in 5 h, to afford roughly an equimolar mixture of the two possible *syn*-addition reaction products, *syn*-(*E*) and *syn*-(*Z*) (entry 4).

Kinetics studies of the terminal alkyne hydrosilylation reaction

The hydrosilylation of 1-hexyne with $HSiMe_2Ph$ catalyzed by [RhBr(CO)(κ^{2}C,N-^{t}BuImCH$_2$PyCH$_2$OMe)] (**6**) proceeded slowly at room temperature but was completed in only 30 min at 333 K (entry 1, Table 1). The reaction was monitored by ^{1}H NMR, using anisole as an internal standard, and the reaction profile showing the evolution of the concentrations of 1-hexyne and of the three vinylsilane isomers (%mol) over time is shown in Fig. 4a. The consumption of 1-hexyne is followed by the gradual formation of the β-(*Z*)-vinylsilane isomer. Although a steady increase in the amount of β-(*E*)- and α-vinylsilane isomers was also observed, the selectivity for the β-(*Z*)-vinylsilane isomer remained approximately constant over the course of the reaction. The ^{1}H NMR spectra did not show the presence of 1-hexene and a GC-MS analysis of an aliquot of the reaction mixture showed only three peaks at *m*/*z* ratio of 218 corresponding to the three vinylsilane isomers, excluding the formation of the dehydrogenative silylation products.

The selectivity in the hydrosilylation of terminal alkynes is influenced by ability of the catalyst to promote isomerization reactions once the reactants have been completely consumed. Thus, both the transformation of the β-(*Z*)-vinylsilane isomer into the more thermodynamically stable β-(*E*) isomer, and the formation of allyl-silyl derivatives in the case of aliphatic alkynes have been previously described in the literature.[1a,6,18,29] The evolution of the β-(*Z*)/β-(*E*) ratio in different hydrosilylation reactions catalyzed by **6** is shown in Fig. 4b. The β-(*Z*) → β-(*E*) vinylsilane isomerization was slow in the case of 1-hexyne hydrosilylation with $HSiMe_2Ph$, as the β-(*Z*)/β-(*E*) ratio of 15.0 observed at the end of the reaction

Table 3 Hydrosilylation of diphenylacetylene and 1-phenyl-1-propyne with $HSiMe_2Ph$ catalyzed by [RhBr(CO)(κ^2*C*,*N*-^{t}BuImCH$_2$PyCH$_2$OMe)] (**6**)[a]

	Silane	Alkyne	Time	Conversion[b] (%)	Selectivity[b] (%)	
					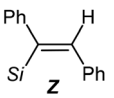 **Z**	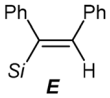 **E**
1	$HSiMe_2Ph$	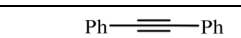	20 min	49	0	100
2			2 h	94	0	100
					Selectivity[b] (%)	
	Silane	Alkyne	Time	Conversion[b] (%)	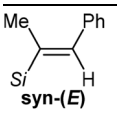 **syn-(*E*)**	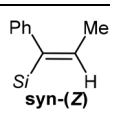 **syn-(*Z*)**
3	$HSiMe_2Ph$	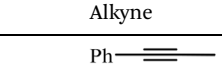	50 min	26	42	58
4			5 h	95	46	54

[a] Reaction conditions: alkyne (0.11 mmol), $HSiMe_2Ph$ (0.11 mmol) and **6** (0.0011 mmol, 1.0 mol%), in $CDCl_3$ (0.5 mL) at 333 K. [b] Conversion, based on $HSiMe_2Ph$ and selectivity determined by ^{1}H-NMR using anisole as internal standard.

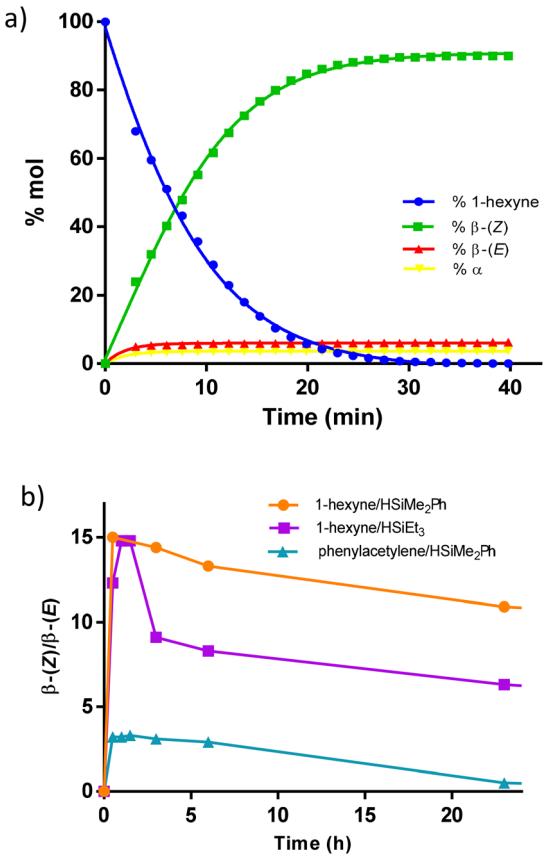

Fig. 4 (a) Reaction profile for the hydrosilylation of 1-hexyne with $HSiMe_2Ph$ monitored by ^1H NMR. (b) Evolution of the β-(*Z*)/β-(*E*) ratio for the hydrosilylation of various alkynes and silanes catalyzed by **6**. Reaction conditions: hydrosilane (0.11 mmol), alkyne (0.11 mmol) and **6** (1 mol%) in $CDCl_3$ (0.5 mL) at 333 K.

(30 min) decreased to 14.4 after 2.5 h and to 10.9 after 24 h. The isomerization rate was higher in the case of the hydrosilylation of 1-hexyne with $HSiEt_3$. The ratio β-(*Z*)/β-(*E*) at the end of the reaction (1.5 h) was 14.8 but it decreased to 9.1 after 3 h and evolved less markedly to 6.3 after 24 h. Finally, the β-(*Z*) → β-(*E*) isomerization was particularly significant in the case of the hydrosilylation of phenylacetylene with $HSiMe_2Ph$. The ratio β-(*Z*)/β-(*E*) of 3.1 at the end of the reaction (3 h) decreased to 0.5 after 24 h (see ESI†). The moderate β-(*Z*) selectivity of 67% for the β-(*Z*)-vinylsilane isomer achieved in the phenylacetylene hydrosilylation is not a consequence of the β-(*Z*) → β-(*E*) isomerization along the reaction, since the same selectivity was obtained after 0.5 h and 1 h with conversions of 57 and 73%, respectively.

The possible influence of the solvent on the catalytic reaction was also investigated. Hydrosilylation of 1-hexyne with $HSiMe_2Ph$ catalyzed by **6** in acetone-d_6 at 323 K was slower than in $CDCl_3$, with 90% conversion in 2 h, and much less selective, 69% to the β-(*Z*)-vinylsilane isomer. Thus, acetone has no positive effect on the catalyst performance and its active participation in the activation of the hydrosilane by an outer sphere mechanism is ruled out.[30] Other non-polar solvents, such as toluene-d_8 or benzene-d_6, were not effective in improving either the activity or the selectivity.

The hydrosilylation of 1-hexyne with $HSiMe_2Ph$ catalyzed by **6** in $CDCl_3$ is highly temperature-dependent, with the catalytic productivity of the β-(*Z*)-vinylsilane increasing with temperature. At 30 °C, the hydrosilylation proceeds up to 92% of conversion in only 80 min with a 87% β-(*Z*) selectivity. The catalytic performance of **6** was studied in the temperature range 30–60 °C in order to determine the activation parameters for the hydrosilylation of 1-hexyne with $HSiMe_2Ph$ in $CDCl_3$ (see ESI†). TOF values determined at 15 min of reaction time (Table 4) were used to calculate the activation parameters by means of an Eyring plot: $\Delta H^{\ddagger}$ = +7.8 ± 1.0 kcal mol^{-1}, $\Delta S^{\ddagger}$ = −40.2 ± 3.3 cal K^{-1} mol^{-1} and $\Delta G^{\ddagger}$ = +19.8 ± 2.0 kcal mol^{-1} at 298 K (Fig. 5 and ESI†).

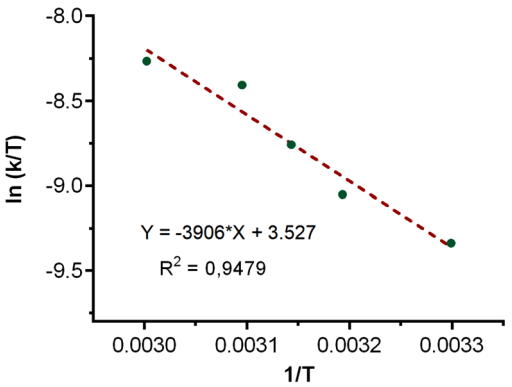

Fig. 5 Eyring plot for the hydrosilylation of 1-hexyne with $HSiMe_2Ph$ catalyzed by **6** in $CDCl_3$.

Table 4 Influence of the temperature in the hydrosilylation of 1-hexyne to β-(*Z*)-hex-1-enyldimethyl(phenyl)silane catalyzed by **6**[a]

Entry	Catalyst	*T* (K)	Conversion[b] (%)	β-(*Z*) Selectivity[b] (%)	TON[c]	TOF[d] (s^{-1})
1	**6**	303	34	71	24	0.02667
2	**6**	313	43	77	33	0.03667
3	**6**	318	53	85	45	0.05000
4	**6**	323	77	84	65	0.07222
5	**6**	333	86	89	77	0.08556

[a] Reaction conditions: 1-hexyne (0.10 mmol), $HSiMe_2Ph$ (0.10 mmol) and **6** (0.001 mmol, 1.0 mol%), in $CDCl_3$ (0.5 mL). [$HSiMe_2Ph$] = [1-hexyne] ≈ 0.22 M. [b] Conversion, based on $HSiMe_2Ph$, and selectivity determined by ^1H NMR after 15 min. [c] TONs for the formation of β-(*Z*)-vinylsilane. [d] TOFs calculated at 15 min.

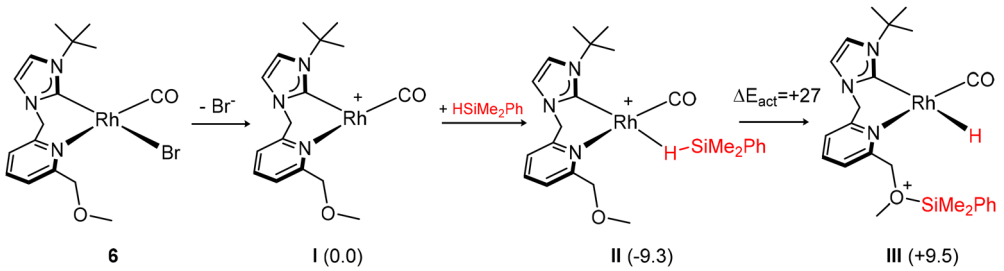

Scheme 3 Calculated reaction sequence for the hydrosilane activation by **6** involving the methoxy fragment of the functionalized lutidine-derived ligand. Relative Gibbs free energies are given in kcal mol^{-1} (B97D3/def2svp, 298 K, 1 atm, CPCM/chloroform).

Mechanistic considerations for the terminal alkyne hydrosilylation reaction catalyzed by 6

Compound [RhBr(CO)(κ^{2}C,N-^{t}BuImCH$_2$PyCH$_2$OMe)] (**6**) does not react with either HSiMe$_2$Ph or 1-hexyne in acetonitrile-d_3 at 333 K for 24 h. However, in the presence of both reagents the hydrosilylation proceeds at room temperature with β-(*Z*) selectivity. DFT calculations were performed in order to assess the possible involvement of the –OMe group in the activation of hydrosilane as the cause of the observed change in stereoselectivity with respect to related rhodium(I) catalysts based on 2-picolyl-functionalized NHC ligands (Scheme 3). The dissociation of the bromido ligand in **6** should lead to the tricoordinate rhodium(I) species (**I**) containing the κ^{2}C, N-^{t}BuImCH$_2$PyCH$_2$OMe ligand and a carbon monoxide ligand. The reaction of **I** with HSiMe$_2$Ph should provide the square planar intermediates **II** containing the coordinated hydrosilane. Intermediate **II** may undergo an –OMe assisted Si–H activation rendering the hydrido derivative **III** featuring an oxonio group resulting from the silylation of the CH$_2$OMe moiety. Notably, the transition state of the transformation **II** → **III** could not be located on the PES, nonetheless the scan of the Si···O coordinate from **II** to **III** revealed that the activation energy for this step (ΔE_{act}) should be around 27 kcal mol^{-1} (see ESI†). Thus, taking into account the above mentioned experimental activation parameters, it can be argued that the direct participation of the –OMe group in the hydrosilane activation should be ruled out.‡

On this basis, hydrosilane activation is likely to proceed *via* a classical Si–H oxidative addition. As a confirmation, the ^{1}H NMR of the mixture resulting from the reaction of **6** with HSi(OEt)$_3$ (20 equiv.), a more reactive hydrosilane, in acetonitrile-d_3 at 333 K for 1 h showed a small high-field doublet at δ −16.64 with a J_{Rh-H} coupling constant of 29.9 Hz, which corresponds to a Rh(III)–H species which could result from the oxidative addition of the hydrosilane to **6** (see ESI†).

A mechanistic proposal based on the classical modified Chalk–Harrod mechanism is depicted in Scheme 4. The proposed key intermediate should result from the Si–H oxidative addition of the hydrosilane followed by the coordination of the alkyne, thus rendering an octahedral rhodium(III) species with the hydrido, silyl and alkyne ligands mutually *cis*-disposed. At this point, silylmetalation of the alkyne by migratory insertion into the Rh–Si bond should occur. 1,2-Alkyne insertion generates the vinylsilane intermediate **A** which, upon reductive elimination and activation of a new hydrosilane molecule, gives rise to the α-isomer and regenerates the catalytic active species. Alternatively, 2,1-alkyne insertion results in the formation of the (*Z*)-silylvinylene rhodium(III) intermediate **B**, which leads to the β-(*E*)-vinylsilane isomer after reductive elim-

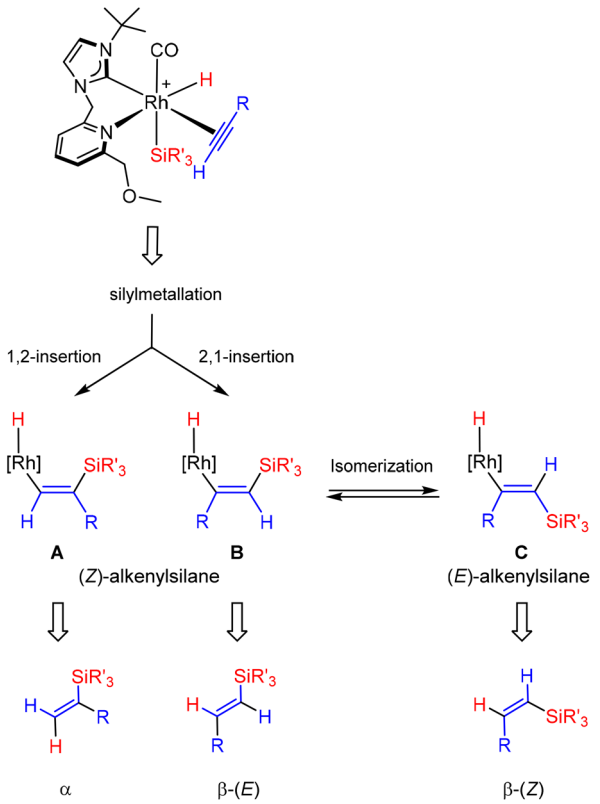

Scheme 4 Proposed modified Chalk–Harrod mechanism for the hydrosilylation of terminal alkynes by **6** leading to the formation of the vinylsilane isomers.

‡Note that although dissociation of the pyridine fragment of the NHC ligand in **6** might also be possible, the formation of the oxonium group would involve a transition state with an 11-membered metallacycle which should be highly unfavorable from an entropic point of view. On this ground, this route has not even explored by DFT calculations.

ination. However, the metal-assisted isomerization of the (*Z*)-silylvinylene intermediate into the thermodynamically more stable (*E*)-silylvinylene complex **C**, *via* a zwitterionic carbene or an η^2-vinyl complex,[31,32] followed by reductive elimination results in the formation of the β-(*Z*)-vinylsilane product. The driving force of the isomerization process is the relief of steric congestion between the metal and the adjacent bulky silane in intermediate **B**. Thus, as the reductive elimination is assumed to be the rate-determining step, the thermodynamically less stable β-(*Z*)-vinylsilane isomer forms as the kinetic product.

As has become apparent in this study, the size and electronic characteristics of the R substituent in the alkyne have a major influence on the selectivity of the hydrosilylation reaction. When the R substituent is not very bulky, as for example in 1-hexyne, the β-(*Z*) isomer selectively forms because the equilibrium between **B** and **C** is expected to shift towards **C**, which allows steric congestion between the metal and the silyl group to be reduced. On the contrary, when the R substituent is bulky, as is the case for 3,3-dimethyl-1-butene, the reaction is not selective. Thus, the R substituent introduces additional steric congestion in **C** and an equilibrium probably establishes between **B** and **C** thereby resulting in the formation of the β-(*Z*) and β-(*E*) vinylsilanes.[6,31] Additionally, the bulkiness of the R group can stabilize the alkenylsilane **A**, with lower steric pressure on the metal centre, from which the α-vinylsilane is obtained.[33]

Conclusions

The neutral compound [RhBr(cod)(κC-^{t}BuImCH$_2$PyCH$_2$OMe)] has been straightforwardly prepared by reaction of the methoxy-functionalized lutidine-derived imidazolium salt [^{t}BuHImCH$_2$PyCH$_2$OMe]Br with [Rh(μ-OMe)(cod)]$_2$. Coordination of the pyridine moiety of the ligand is induced by abstraction of the bromido ligand to afford the cationic compound [Rh(cod)(κ^{2}C,N-^{t}BuImCH$_2$PyCH$_2$OMe)]PF$_6$. Carbonylation of the latter affords the dicarbonyl compound [Rh(CO)$_2$(κ^{2}C,N-^{t}BuImCH$_2$PyCH$_2$OMe)]PF$_6$ whereas carbonylation of the neutral compound affords a mixture of di- and monocarbonyl neutral complexes [RhBr(CO)$_2$(κC-^{t}BuImCH$_2$PyCH$_2$OMe)] and [RhBr(CO)(κ^{2}C,N-^{t}BuImCH$_2$PyCH$_2$OMe)] which can be separated due to their different solubility. All these complexes efficiently catalyzed the hydrosilylation of 1-hexyne with HSiMe$_2$Ph, showing selectivity towards the β-(*Z*)-vinylsilane product. Among these, the unusual compound [RhBr(CO)(κ^{2}C,N-^{t}BuImCH$_2$PyCH$_2$OMe)] gives the best results in activity and selectivity. This catalyst has been successfully applied to the hydrosilylation of a range of terminal and internal alkynes with a variety of hydrosilanes having different steric properties. It has been observed that the selectivity depends on the steric and electronic characteristics of the alkyne. In general, excellent β-(*Z*) selectivity has been observed in the hydrosilylation of linear aliphatic 1-alkynes even with bulky hydrosilanes, although for very bulky hydrosilanes, such as HSiPh$_3$, the activity decreases dramatically. The hydrosilylation of phenylacetylene derivatives, 2-ethynylpyridine or 3-phenyl-1-propyne, also proceeds efficiently although with moderate selectivity to the β-(*Z*)-vinylsilane product. In contrast, the hydrosilylation of the bulky 3,3-dimethyl-1-butyne was unselective. Compound [RhBr(CO)(κ^{2}C,N-^{t}BuImCH$_2$PyCH$_2$OMe)] catalyzes the β-(*Z*) → β-(*E*) vinylsilane isomerization, the rate of this process being faster with aromatic alkynes than with aliphatic alkynes. On the other hand, the hydrosilylation of internal alkynes proceeds with complete selectivity towards the *syn*-addition vinylsilane products.

The β-(*Z*) selectivity of these catalysts, featuring a methoxymethyl functionality in close proximity to the rhodium centre, contrasts with that of related rhodium(I) catalysts based on 2-picolyl-functionalised NHC ligands which were reported to be β-(*E*) selective. The possible involvement of the methoxymethyl fragment in the activation of hydrosilane as the cause of the observed change in stereoselectivity has been investigated by DFT calculations. The calculated energy barrier for this process is higher than the determined from experimental kinetic studies, $\Delta G^{\ddagger}$ of 19.8 ± 2.0 kcal mol^{-1} (298 K), suggesting that hydrosilane activation is likely to proceed *via* a classical Si–H oxidative addition. However, possible involvement of the –OMe group in the key isomerization of the (*Z*)-silylvinylene intermediate and/or the activation/insertion of the incoming alkyne cannot be excluded.

Experimental section

General considerations

All reactions were carried out with rigorous exclusion of air using Schlenk-tube techniques or glovebox. Organic solvents were dried by standard methods and distilled under argon prior to use or obtained oxygen- and water-free from a Solvent Purification System (Innovative Technologies). The starting materials [Rh(μ-Cl)(cod)]$_2$ [34] and [Rh(μ-OMe)(cod)]$_2$ [35] were prepared as previously described in the literature. The imidazolium salt [^{t}BuHImCH$_2$PyCH$_2$OMe]Br (**1**)[24] was prepared following the procedure recently described by us. Deuterated solvents (Euriso-top) $CDCl_3$ and C_6D_6 were dried using activated molecular sieves.

Scientific equipment

C, H, and N analyses were carried out in a PerkinElmer 2400 Series II CHNS/O analyzer. Infrared spectra were recorded on a 100 FTIR-PerkinElmer Spectrophotometer equipped with a Universal Attenuated Total Reflectance (UATR) accessory. ^{1}H and ^{13}C{^{1}H} NMR spectra were recorded on a Bruker Avance 300 (300.1276 MHz and 75.4792 MHz). Chemical shifts are reported in ppm relative to tetramethylsilane and coupling constants (*J*) are given in Hertz (Hz). Spectral assignments were achieved by combination of ^{1}H–^{1}H COSY, ^{13}C APT, ^{1}H–^{13}C HSQC and ^{1}H–^{13}C HMBC experiments. High-resolution electrospray ionization mass spectra (HRMS-ESI) were recorded using a Bruker MicroToF-Q equipped with an API-ESI source and a Q-ToF mass analyzer, which leads a maximum error in the measurement of 5 ppm, using sodium formate as refer-

ence. Conductivities were measured in *ca.* 5×10^{-4} M nitromethane solutions of the complexes using a Philips PW 9501/01 conductimeter.

Synthesis of [RhBr(cod)(κC-^{t}BuImCH$_2$PyCH$_2$OMe)] (2)

[Rh(μ-OMe)(cod)]$_2$ (142 mg, 0.294 mmol) was added to a solution of [^{t}BuHImCH$_2$PyCH$_2$OMe]Br (**1**) (200 mg, 0.588 mmol) in dichloromethane (5 mL) and stirred for 15 h at room temperature. The resulting yellow solution was brought to dryness under vacuum to give an oily residue that was disaggregated by stirring with cold pentane. The solid was filtered, washed with pentane (2 × 5 mL) and dried under vacuum. Yield: 312 mg, 96% (pale yellow solid). Anal. calcd for $C_{23}H_{33}BrN_3ORh$: C, 50.20; H, 6.04; N, 7.63. Found: C, 50.33; H, 6.01; N, 7.55. HRMS (ESI$^+$, MeOH, *m*/*z*): calcd for $C_{23}H_{33}BrN_3ORh$, 549.0862; found, 470.1673 [M − Br]$^+$. ^{1}H NMR (298 K, 300 MHz, C_6D_6): δ 7.68 (d, J_{H-H} = 7.4 Hz, 1H, H$_m$ Py), 7.22–7.13 (m, 2H, H$_m$ and H$_p$ Py), 6.91 (d, J_{H-H} = 14.6 Hz, 1H, CH$_2$Im), 6.54 (d, J_{H-H} = 2.1 Hz, 1H, =CH Im), 6.36 (d, J_{H-H} = 2.1 Hz, 1H, =CH Im), 5.99 (d, J_{H-H} = 14.7 Hz, 1H, CH$_2$Im), 5.52 (m, 1H, =CH cod), 5.45 (m, 1H, =CH cod), 4.53 (ABq, δ_A = 4.56, δ_B = 4.50 J_{A-B} = 4.0 Hz, 2H, CH$_2$OMe), 3.43 (m, 1H, =CH cod), 3.30 (m, 1H, =CH cod), 3.16 (s, 3H, OCH$_3$), 2.37–2.01 (m, 4H, >CH$_2$ cod), 1.73 (s, 9H, ^{t}Bu), 1.71–1.51 (m, 4H, >CH$_2$ cod). ^{13}C{^{1}H} NMR (298 K, 75 MHz, C_6D_6): δ 182.3 (d, J_{Rh-C} = 50.1 Hz, C$_{NCN}$), 158.5, 156.2 (C$_o$ Py), 137.4 (C$_p$ Py), 122.5 (C$_m$ Py), 120.1 (=CH Im), 120.1 (C$_m$ Py), 119.9 (=CH Im), 96.0 (d, J_{Rh-C} = 7.5 Hz, =CH cod$_{trans\text{-}NHC}$), 93.8 (d, J_{Rh-C} = 7.3 Hz, =CH cod$_{trans\text{-}NHC}$), 75.5 (CH$_2$OMe), 70.6 (d, J_{Rh-C} = 15.1 Hz, =CH cod$_{trans\text{-}Br}$), 67.8 (d, J_{Rh-C} = 14.1 Hz, =CH cod$_{trans\text{-}Br}$), 58.4 (CH$_2$Im), 58.2 (OCH$_3$), 58.1 (C ^{t}Bu), 33.2 (>CH$_2$ cod), 31.7 (CH$_3$ ^{t}Bu), 31.6 (>CH$_2$ cod), 29.8 (>CH$_2$ cod), 28.7 (>CH$_2$ cod).

Synthesis of [Rh(cod)(κ^{2}C,N-^{t}BuImCH$_2$PyCH$_2$OMe)]PF$_6$ (3)

AgPF$_6$ (92 mg, 0.364 mmol) was added to a solution of [RhBr(cod)(^{t}BuImCH$_2$PyCH$_2$OMe)] (**2**) (200 mg, 0.360 mmol) in dichloromethane (5 mL). The suspension was stirred at room temperature for 30 min, filtered through Celite to remove the silver bromide formed, and washed with dichloromethane (2 × 5 mL). The solution was brought to dryness under vacuum to give an oily residue which was disaggregated by stirring with cold diethyl ether. The solid was filtered, washed with diethyl ether (2 × 5 mL) and dried under vacuum. Yield: 212 mg, 96% (pale yellow solid). Anal. calcd for $C_{23}H_{33}F_6N_3OPRh$: C, 44.89; H, 5.40. Found: C, 44.70; H, 5.65; N, 6.48. HRMS (ESI$^+$, MeOH, *m*/*z*): calcd for $C_{23}H_{33}N_3ORh$, 470.1679; found, 470.1679 [M]$^+$. Λ_M (nitromethane, 5.0×10^{-4} M) = 78 Ω^{-1} cm^2 mol^{-1}. ^{1}H NMR (298 K, 300 MHz, $CDCl_3$): δ 7.91–7.80 (m, 2H, H$_m$ and H$_p$ Py), 7.46 (d, J_{H-H} = 2.0 Hz, 1H, =CH Im), 7.34 (d, J_{H-H} = 7.7 Hz, 1H, H$_m$ Py), 6.90 (d, J_{H-H} = 2.3 Hz, 1H, =CH Im), 6.52 (d, J_{H-H} = 14.9 Hz, 1H, CH$_2$Im), 5.76 (d, J_{H-H} = 14.9 Hz, 1H, CH$_2$Im), 4.63 (ABq, δ_A = 4.72, δ_B = 4.54 J_{A-B} = 4.5 Hz, 2H, CH$_2$OMe), 4.44 (m, 1H, =CH cod), 4.25 (m, 1H, =CH cod), 3.99 (m, 1H, =CH cod), 3.85 (m, 1H, =CH cod), 3.58 (s, 3H, OCH$_3$), 2.60–2.23 (m, 4H, >CH$_2$ cod), 2.18–1.82 (m, 4H, >CH$_2$ cod), 1.71 (s, 9H, ^{t}Bu). ^{31}P{^{1}H} NMR (298 K, 121.4 MHz, $CDCl_3$): δ −144.0 (sept). ^{13}C{^{1}H} NMR (298 K, 75 MHz, $CDCl_3$): δ 175.5 (d, J_{Rh-C} = 49.5 Hz, C$_{NCN}$), 158.8, 155.2 (C$_o$ Py), 139.4 (C$_p$ Py), 124.9, 124.0 (C$_m$ Py), 122.9, 119.0 (=CH Im), 98.7 (d, J_{Rh-C} = 8.4 Hz, =CH cod$_{trans\text{-}NHC}$), 92.7 (d, J_{Rh-C} = 7.0 Hz, =CH cod$_{trans\text{-}NHC}$), 75.1 (CH$_2$OMe), 74.8 (d, J_{Rh-C} = 15.4 Hz, =CH cod$_{trans\text{-}Py}$), 68.8 (d, J_{Rh-C} = 13.1 Hz, =CH cod$_{trans\text{-}Py}$), 59.3 (OCH$_3$), 59.0 (C ^{t}Bu), 58.1 (CH$_2$Im), 32.1 (>CH$_2$ cod), 31.9 (CH$_3$ ^{t}Bu), 29.8 (>CH$_2$ cod), 29.0 (>CH$_2$ cod), 28.7 (>CH$_2$ cod).

Synthesis of [Rh(CO)$_2$(κ^{2}C,N-^{t}BuImCH$_2$PyCH$_2$OMe)]PF$_6$ (4)

Carbon monoxide was bubbled through a solution of [Rh(cod)(κ^{2}C,N-^{t}BuImCH$_2$PyCH$_2$OMe)]PF$_6$ (**3**) (100 mg, 0.162 mmol) in dichloromethane (5 mL) for 5 min to give a yellow solution. The solution was brought to dryness under vacuum to give an oily residue which was disaggregated by stirring with cold hexane. The solid was filtered, washed with hexane (2 × 5 mL) and dried under vacuum. Yield: 71 mg, 78% (yellow solid). Anal. calcd for $C_{17}H_{21}F_6N_3O_3PRh$: C, 36.25; H, 3.76; N, 7.46. Found: C, 36.64; H, 3.59; N, 7.01. HRMS (ESI$^+$, MeOH, *m*/*z*): calc. for $C_{17}H_{21}N_3O_3Rh$, 418.0638; found, 390.0681 [M − CO]$^+$, 362.0792 [M − 2CO]$^+$. IR (ATR, cm^{-1}): 2081, 2008 (ν_{CO}). Λ_M (nitromethane, 5.0×10^{-4} M) = 77 Ω^{-1} cm^2 mol^{-1}. ^{1}H NMR (298 K, 300 MHz, $CDCl_3$): δ 8.04–7.95 (m, 2H, H$_p$ and H$_m$ Py), 7.60 (d, J_{H-H} = 2.0 Hz, 1H, =CH Im), 7.56 (d, J_{H-H} = 7.2 Hz, 1H, H$_m$ Py), 7.17 (d, J_{H-H} = 2.0 Hz, 1H, =CH Im), 5.75 (ABq, δ_A = 5.77, δ_B = 5.73 J_{A-B} = 5.0 Hz, 2H, CH$_2$Im), 4.67 (ABq, δ_A = 4.73, δ_B = 4.71 J_{A-B} = 4.0 Hz, 2H, CH$_2$OMe), 3.54 (s, 3H, OCH$_3$), 1.76 (s, 9H, ^{t}Bu). ^{31}P{^{1}H} NMR (298 K, 121.4 MHz, $CDCl_3$): δ −144.2 (sept). ^{13}C{^{1}H} NMR (298 K, 75 MHz, $CDCl_3$): δ 185.8 (d, J_{Rh-C} = 74.0 Hz, CO$_{trans\text{-}Py}$), 184.6 (d, J_{Rh-C} = 55.9 Hz, CO$_{trans\text{-}NHC}$), 168.9 (d, J_{Rh-C} = 43.7 Hz, C$_{NCN}$), 159.4, 154.9 (C$_o$ Py), 141.8 (C$_p$ Py), 126.2, 124.9 (C$_m$ Py), 123.7, 120.3 (=CH, Im), 75.8 (CH$_2$OMe), 59.4 (OCH$_3$), 59.2 (C ^{t}Bu), 56.9 (CH$_2$Im), 31.9 (CH$_3$ ^{t}Bu).

Synthesis of [RhBr(CO)$_2$(κC-^{t}BuImCH$_2$PyCH$_2$OMe)] (5)

Carbon monoxide was bubbled through a solution of [RhBr(cod)(κC-^{t}BuImCH$_2$PyCH$_2$OMe)] (**2**) (100 mg, 0.182 mmol) in dichloromethane (2 mL) until complete evaporation of the solvent. The oily residue was disaggregated by stirring with cold hexane to give a yellow solid which was filtered, washed with hexane (2 × 5 mL) and dried by prolonged exposure to a stream of CO. Yield: 85 mg, 94% (yellow solid). Anal. calcd for $C_{17}H_{21}BrN_3O_3Rh$: C, 40.99; H, 4.25; N, 8.44. Found: C, 41.17; H, 4.41; N, 8.43. HRMS (ESI$^+$, MeOH, *m*/*z*): calc. for $C_{17}H_{21}BrN_3O_3Rh$, 496.9821; found, 362.0766 [M − 2CO − Br]$^+$. IR (ATR, cm^{-1}): 2066, 1988 (ν_{CO}). ^{1}H NMR (298 K, 300 MHz, $CDCl_3$): δ 7.69 (t, J_{H-H} = 7.7 Hz, 1H, H$_p$ Py), 7.37 (d, J_{H-H} = 7.7 Hz, 1H, H$_m$ Py), 7.32 (d, J_{H-H} = 7.8 Hz, 1H, H$_m$ Py), 7.19 (d, J_{H-H} = 1.8 Hz, 1H, =CH Im), 7.13 (d, J_{H-H} = 1.9 Hz, 1H, =CH Im), 5.80 (ABq, δ_A = 5.92, δ_B = 5.69 J_{A-B} = 15.0 Hz, 2H, CH$_2$Im), 4.56 (s, 2H, CH$_2$OMe), 3.48 (s, 3H, OCH$_3$), 1.82 (s, 9H, ^{t}Bu). ^{13}C{^{1}H} NMR (298 K, 75 MHz, $CDCl_3$): δ 186.1 (d, J_{Rh-C} = 54.1 Hz, CO$_{trans\text{-}NHC}$), 182.4 (d, J_{Rh-C} = 77.8 Hz, CO$_{trans\text{-}Br}$), 172.3 (d, J_{Rh-C} = 41.6 Hz, C$_{NCN}$) 158.7, 154.9 (C$_o$ Py), 137.7 (C$_p$ Py), 122.0 (C$_m$ Py), 121.5 (=CH, Im), 120.8 (C$_m$ Py), 120.3 (=CH, Im), 75.5 (CH$_2$OMe), 66.0 (C ^{t}Bu) 59.0 (OCH$_3$), 58.1 (CH$_2$Im), 32.3 (CH$_3$ ^{t}Bu).

Synthesis of [RhBr(CO)(κ²C,N-^{t}BuImCH$_2$PyCH$_2$OMe)] (6)

Carbon monoxide was bubbled through a solution of [RhBr(cod)(κC-^{t}BuImCH$_2$PyCH$_2$OMe)] (**2**) (100 mg, 0.182 mmol) in dichloromethane (10 mL) for 5 min to give a pale yellow solution. The solution was brought to dryness under vacuum to give an oily residue obtained which was partially dissolved by addition of diethyl ether (2 × 5 mL). The suspension was filtered and washed with diethyl ether (2 × 5 mL). The obtained solution was brought to dryness under vacuum yielding the compound as a pale-yellow solid. Yield: 42 mg, 49% (yellow solid). Anal. calcd for $C_{16}H_{21}BrN_3O_2Rh$: C, 40.87; H, 4.50; N, 8.94. Found: C, 40.42; H, 4.66; N, 8.84. HRMS (ESI$^+$, MeOH, *m*/*z*): calc. for $C_{16}H_{21}BrN_3O_2Rh$, 468.9872; found, 390.0683 [M − Br]$^+$. IR (ATR, cm^{-1}): 1963 (ν_{CO}). ^{1}H NMR (298 K, 300 MHz, $CDCl_3$): δ 7.73 (t, J_{H-H} = 7.8 Hz, 1H, H$_p$ Py), 7.51 (d, J_{H-H} = 7.8 Hz, 1H, H$_m$ Py), 7.30 (d, J_{H-H} = 7.2 Hz, 1H, H$_m$ Py), 7.05 (d, J_{H-H} = 1.9 Hz, 1H, =CH Im), 7.02 (d, J_{H-H} = 1.8 Hz, 1H, =CH Im), 6.47 (d, J_{H-H} = 14.3 Hz, 1H, CH_2Im), 5.49 (d, J_{H-H} = 14.4 Hz, 1H, CH_2OMe), 5.02 (d, J_{H-H} = 14.4 Hz, 1H, CH_2Im), 4.93 (d, J_{H-H} = 14.4 Hz, 1H, CH_2OMe), 3.50 (s, 3H, OCH_3), 1.88 (s, 9H, ^{t}Bu). ^{13}C{^{1}H} NMR (298 K, 75 MHz, $CDCl_3$): δ 191.2 (d, J_{Rh-C} = 34.6 Hz, CO), 176.4 (d, J_{Rh-C} = 38.7 Hz, C_{NCN}), 163.5, 153.8 (C$_o$ Py), 138.9 (C$_p$ Py), 123.1, 121.6 (C$_m$ Py), 119.9, 118.6 (=CH, Im), 77.0 (CH_2OMe), 59.4 (OCH_3), 58.9 (C ^{t}Bu), 57.3 (CH_2Im), 31.7 (CH_3 ^{t}Bu).

Catalytic hydrosilylation reactions

Hydrosilylation catalytic tests were carried out in NMR tubes under argon atmosphere. In a typical procedure, an NMR tube was charged under argon with the catalyst (0.0011 mmol), $CDCl_3$ (0.5 mL), anisole as internal standard (0.009 mmol), hydrosilane (0.11 mmol) and alkyne (0.11 mmol). The solution was kept at room temperature or in a thermostated bath at 333 K and monitored by ^{1}H NMR spectroscopy. The vinylsilane reaction products were unambiguously characterized on the basis of the $^3J_{H-H}$ coupling constants of the vinylic protons in the NMR spectra and subsequent comparison to literature data. Values of *J* ranged from 17 to 19 Hz for β-(*E*), 13 to 16 Hz for β-(*Z*), and 1 to 3 Hz for α-vinylsilanes.[6,36] Yields and selectivities were determined by ^{1}H NMR spectroscopy.

Crystal structure determination

Single crystals of **2** were obtained by cooling a saturated solution of the compound in toluene at 278 K. Single crystals suitable for the X-ray diffraction studies were grown by slow diffusion of diethyl ether and hexane into a concentrated solution of the complexes in acetone (**3**) and dichloromethane (**6**), respectively. X-ray diffraction data were collected at 100(2) K on a Bruker APEX DUO (**2**, **3**) or APEX SMART (**6**) diffractometer with graphite-monochromated Mo-Kα radiation (λ = 0.71073 Å) using <1° ω rotations. Intensities were integrated and corrected for absorption effects with SAINT-PLUS[37] and SADABS[38] programs, both included in APEX2 package. The structures were solved by the Patterson method with SHELXS-97 [39] and refined by full matrix least-squares on F^2 with SHELXL-2014,[40] under WinGX.[41] Pitch and yaw angles were calculated according to the literature.[42]

Crystal data and structure refinement for 2

$C_{23}H_{33}BrN_3ORh$, 550.34 g mol^{-1}, monoclinic, $P2_1/c$, a = 8.5969(9) Å, b = 11.0481(11) Å, c = 24.128(2) Å, β = 98.620(2)°, V = 2265.7(4) Å^3, Z = 4, $D_{calc.}$ = 1.613 g cm^{-3}, μ = 2.536 mm^{-1}, F(000) = 1120, yellow prism, 0.160 × 0.140 × 0.060 mm^3, θ_{min}/θ_{max} 1.707/29.620°, index ranges −11 ≤ h ≤ 11, −15 ≤ k ≤ 14, −33 ≤ l ≤ 26, reflections collected/independent 35 831/6056 [R(int) = 0.0411], data/restraints/parameters 6056/0/266, GooF(F^2) = 1.045, R_1 = 0.0287 [$I > 2\sigma(I)$], wR_2 = 0.0691 (all data), largest diff. peak/hole 1.499/−0.590 e Å^{-3}. CCDC deposit number 2248982.†

Crystal data and structure refinement for 3

$C_{23}H_{33}F_6N_3OPRh$, 615.40 g mol^{-1}, triclinic, $P\bar{1}$, a = 9.7280(13) Å, b = 11.3893(15) Å, c = 12.1763(16) Å, α = 104.166(2)°, β = 104.253(2)°, γ = 100.643(2)°, V = 1224.0(3) Å^3, Z = 2, $D_{calc.}$ = 1.670 g cm^{-3}, μ = 0.831 mm^{-1}, F(000) = 628, yellow prism, 0.155 × 0.120 × 0.085 mm^3, θ_{min}/θ_{max} 1.812/29.605°, index ranges −13 ≤ h ≤ 13, −15 ≤ k ≤ 15, −16 ≤ l ≤ 16, reflections collected/independent 13 271/6215 [R(int) = 0.0231], data/restraints/parameters 6215/2/320, GooF(F^2) 1.034, R_1 = 0.0284 [$I > 2\sigma(I)$], wR_2 = 0.0682 (all data), largest diff. peak/hole 0.736/−0.637 e Å^{-3}. CCDC deposit number 2248981.†

Crystal data and structure refinement for 6

$C_{32}H_{42}Br_2N_6O_4Rh_2$, 940.35 g mol^{-1}, monoclinic, $P2_1/n$, a = 11.9388(8) Å, b = 9.9973(7) Å, c = 14.8252(10) Å, β = 107.1460(10)°, V = 1690.8(2) Å^3, Z = 2, $D_{calc.}$ = 1.847 g cm^{-3}, μ = 3.386 mm^{-1}, F(000) = 936, yellow prism, 0.220 × 0.095 × 0.075 mm^3, θ_{min}/θ_{max} 2.494/28.538°, index ranges −15 ≤ h ≤ 15, −13 ≤ k ≤ 13, −19 ≤ l ≤ 19, reflections collected/independent 19 228/4097 [R(int) = 0.0385], data/restraints/parameters 4097/0/212, GooF(F^2) = 1.048, R_1 = 0.0321 [$I > 2\sigma(I)$], wR_2 = 0.0801 (all data), largest diff. peak/hole 0.667/−1.196 e Å^{-3}. CCDC deposit number 2248980.†

DFT calculations

Molecular structure optimizations and frequencies calculations were carried out with the Gaussian16 (revision C.01)[43] using the method B97D3, including the D3 dispersion correction scheme by Grimme with Becke–Johnson damping.[44] The def2-SVP[45] basis and pseudo potential, if applicable, were used for all atoms and the "ultrafine" grid was employed in all calculations. Stationary points were characterized by vibrational analysis. The structures were optimized in chloroform (298 K, 1 atm) using the CPCM method.[46]

Author contributions

The manuscript was written through contributions of all authors. All authors have given approval to the final version of the manuscript.

Conflicts of interest

The authors declare no competing financial interest.

Acknowledgements

The authors express their appreciation for the financial support from the Spanish Ministerio de Ciencia e Innovación, MCIN/AEI/10.13039/501100011033, under the project PID2019-103965GB-I00, and the "Departamento de Ciencia, Universidad y Sociedad del Conocimiento del Gobierno de Aragón" (group E42_23R).

Notes and references

1 (*a*) D. M. P. Mingos and R. H. Crabtree, *Comprehensive Organometallic Chemistry III*, Elsevier, Amsterdam, 2007; (*b*) Z. Rappoport and Y. Apeloig, *The Chemistry of Organic Silicon Compounds*, Wiley, Chichester, 1998.

2 (*a*) R. J. Hofmann, M. Vlatkovic and F. Wiesbrock, *Polymers*, 2017, **9**, 534–571; (*b*) D. Wang, Z. Zhang, Y. Li and C. Xu, *ACS Appl. Mater. Interfaces*, 2014, **6**, 10014–10021; (*c*) H. Liu, B. Fu, Y. Li, Q. Shang and G. J. Xiao, *Coat. Technol. Res.*, 2013, **10**, 361–369; (*d*) G. B. Zhang, J. Kong, X. D. Fan, X. G. Li, W. Tian and M. R. Huang, *Appl. Organomet. Chem.*, 2009, **23**, 277–282.

3 (*a*) R. Hua, *Addition Reactions with Unsaturated Hydrocarbons*, Wiley-VCH, Weinheim, 2022; (*b*) B. M. Trost and Z. T. Ball, *Synthesis*, 2005, 853–887.

4 L. H. Sommer, E. W. Pietrusza and F. C. Whitmore, *J. Am. Chem. Soc.*, 1947, **69**, 188–188.

5 (*a*) M. Zaranek and P. Pawluc, *ACS Catal.*, 2018, **8**, 9865–9876; (*b*) J. Sun and L. Deng, *ACS Catal.*, 2016, **6**, 290–300; (*c*) B. Marciniec, *Coord. Chem. Rev.*, 2005, **249**, 2374–2390; (*d*) Y. Nakajima and S. Shimada, *RSC Adv.*, 2015, **5**, 20603–20616; (*e*) D. Troegel and J. Stohrer, *Coord. Chem. Rev.*, 2011, **255**, 1440–1459; (*f*) B. Marciniec, *Hydrosilylation: A Comprehensive Review on Recent Advances*, Springer, New York, 2009.

6 J. J. Pérez-Torrente, D. H. Nguyen, M. V. Jiménez, F. J. Modrego, R. Puerta-Oteo, D. Gómez-Bautista, M. Iglesias and L. A. Oro, *Organometallics*, 2016, **35**, 2410–2422.

7 (*a*) P. Bellotti, M. Koy, M. N. Hopkinson and F. Glorius, *Nat. Rev. Chem.*, 2021, **5**, 711–725; (*b*) E. Peris, *Chem. Rev.*, 2018, **118**, 9988–10031; (*c*) A. Vivancos, C. Segarra and M. Albrecht, *Chem. Rev.*, 2018, **118**, 9493–9586; (*d*) *N-Heterocyclic Carbenes: Effective Tools for Organometallic Synthesis*, ed. S. P. Nolan, Wiley-VCH, Weinheim, 2014.

8 (*a*) W. Gao and S. Ding, *Synthesis*, 2020, 3549–3563; (*b*) S. Díez-González, N. Marion and S. P. Nolan, *Chem. Rev.*, 2009, **109**, 3612–3676; (*c*) V. Dragutan, I. Dragutan, L. Delaude and A. Demonceau, *Coord. Chem. Rev.*, 2007, **251**, 765–794.

9 L. D. De Almeida, H. Wang, K. Junge, X. Cui and M. Beller, *Angew. Chem., Int. Ed.*, 2021, **60**, 550–565.

10 (*a*) G. Berthon-Gelloz, J.-M. Schumers, G. De Bo and I. E. Markó, *J. Org. Chem.*, 2008, **73**, 4190–4197; (*b*) G. De Bo, G. Berthon-Gelloz, B. Tinant and I. E. Markó, *Organometallics*, 2006, **25**, 1881–1890; (*c*) I. E. Markó, S. Stérin, O. Buisine, G. Mignani, P. Branlard, B. Tinant and J.-P. Declercq, *Science*, 2002, **298**, 204–206.

11 T. K. Meister, K. Riener, P. Gigler, J. Stohrer, W. A. Herrmann and F. E. Kühn, *ACS Catal.*, 2016, **6**, 1274–1284.

12 E. Mas-Marzá, M. Sanaú and E. Peris, *Inorg. Chem.*, 2005, **44**, 9961–9967.

13 M. O. Karataş, B. Alıcı, V. Passarelli, I. Özdemir, J. J. Pérez-Torrente and R. Castarlenas, *Dalton Trans.*, 2021, **50**, 11206–11215.

14 A. Zanardi, E. Peris and J. A. Mata, *New J. Chem.*, 2008, **32**, 120–126.

15 (*a*) B. Sánchez-Page, M. V. Jiménez, J. J. Pérez-Torrente, V. Passarelli, J. Blasco, G. Subias, M. Granda and P. Álvarez, *ACS Appl. Nano Mater.*, 2020, **3**, 1640–1655; (*b*) B. Sánchez-Page, J. Munarriz, M. V. Jiménez, J. J. Pérez-Torrente, J. Blasco, G. Subias, V. Passarelli and A. Álvarez, *ACS Catal.*, 2020, **10**, 13334–13351.

16 P. K. R. Panyam, B. Atwi, F. Ziegler, W. Frey, M. Nowakowski, M. Bauer and M. R. Buchmeiser, *Chem. – Eur. J.*, 2021, **27**, 17220–17229.

17 M. V. Jiménez, J. J. Pérez-Torrente, M. I. Bartolomé, V. Gierz, F. J. Lahoz and L. A. Oro, *Organometallics*, 2008, **27**, 224–234.

18 (*a*) L. Busetto, M. C. Cassani, C. Femoni, M. Mancinelli, A. Mazzanti, R. Mazzoni and G. Solinas, *Organometallics*, 2011, **30**, 5258–5272; (*b*) M. C. Cassani, M. A. Brucka, C. Femoni, M. Mancinelli, A. Mazzanti, R. Mazzoni and G. Solinas, *New J. Chem.*, 2014, **38**, 1768–1779.

19 J. P. Morales-Cerón, P. Lara, J. López-Serrano, L. L. Santos, V. Salazar, E. Álvarez and A. Suárez, *Organometallics*, 2017, **36**, 2460–2469.

20 A. Tyagi, S. Yadav, P. Daw, C. Ravi and J. K. Bera, *Polyhedron*, 2019, **172**, 167–174.

21 S. Hameury, P. De Frémont and P. Braunstein, *Chem. Soc. Rev.*, 2017, **46**, 632–733.

22 (*a*) H. Türkmen, T. Pape, F. E. Hahn and B. Çetinkaya, *Eur. J. Inorg. Chem.*, 2008, 5418–5423; (*b*) A. Binobaid, M. Iglesias, D. Beetstra, A. Dervisi, I. Fallis and K. J. Cavell, *Eur. J. Inorg. Chem.*, 2010, 5426–5431; (*c*) M. V. Jiménez, J. Fernández-Tornos, F. J. Modrego, J. J. Pérez-Torrente and L. A. Oro, *Chem. – Eur. J.*, 2015, **21**, 17877–17889; (*d*) M. V. Jiménez, J. Fernández-Tornos, M. González-Lainez, B. Sánchez-Page, F. J. Modrego, L. A. Oro and J. J. Pérez-Torrente, *Catal. Sci. Technol.*, 2018, **8**, 2381–2393.

23 M. Angoy, M. V. Jiménez, F. J. Lahoz, E. Vispe and J. J. Pérez-Torrente, *Polym. Chem.*, 2022, **13**, 1411–1421.

24 (*a*) M. González-Lainez, M. V. Jiménez, V. Passarelli and J. J. Pérez-Torrente, *Catal. Sci. Technol.*, 2020, **10**, 3458–3467; (*b*) M. González-Lainez, M. V. Jiménez, R. Azpiroz,

V. Passarelli, F. J. Modrego and J. J. Pérez-Torrente, *Organometallics*, 2022, **41**, 1364–1380.

25 (*a*) V. Diachenko, M. J. Page, M. R. D. Gatus, M. Bhadbhade and B. A. Messerle, *Organometallics*, 2015, **34**, 4543–4552; (*b*) W. A. Herrmann, J. Schütz, G. D. Frey and E. Herdtweck, *Organometallics*, 2006, **25**, 2437–2448.

26 (*a*) M. Poyatos, A. Maisse-François, S. Bellemin-Laponnaz and L. H. Gade, *Organometallics*, 2006, **25**, 2634–2641; (*b*) V. César, S. Bellemin-Laponnaz and L. H. Gade, *Eur. J. Inorg. Chem.*, 2004, 3436–3444.

27 (*a*) M. Angoy, M. V. Jiménez, F. J. Lahoz, E. Vispe and J. J. Pérez-Torrente, *Polym. Chem.*, 2022, **13**, 1411–1421; (*b*) Y. Wang, W. Wang, X. Wang, X. Cheng, A. Qin, J. Z. Sun and B. Z. Tang, *Polym. Chem.*, 2017, **8**, 5546–5553; (*c*) M. V. Jiménez, J. J. Pérez-Torrente, M. I. Bartolomé, E. Vispe, F. J. Lahoz and L. A. Oro, *Macromolecules*, 2009, **42**, 8146–8156.

28 Z. Mazloomi, R. Pretorius, O. Pàmies, M. Albrecht and M. Diéguez, *Inorg. Chem.*, 2017, **56**, 11282–11298.

29 L. Yong, K. Kirleis and H. Butenschön, *Adv. Synth. Catal.*, 2006, **348**, 833–836.

30 M. Iglesias, P. J. Sanz Miguel, V. Polo, F. J. Fernández-Álvarez, J. J. Pérez-Torrente and L. A. Oro, *Chem. – Eur. J.*, 2013, **19**, 17559–17566.

31 (*a*) C. H. Jun and R. H. Crabtree, *J. Organomet. Chem.*, 1993, **447**, 177–187; (*b*) R. S. Tanke and R. H. Crabtree, *J. Am. Chem. Soc.*, 1990, **112**, 7984–7989.

32 (*a*) I. Ojima and M. Kumagai, *J. Organomet. Chem.*, 1974, **66**, C12–C14; (*b*) I. Ojima, N. Clos, R. J. Donovan and P. Ingallina, *Organometallics*, 1990, **9**, 3127–3133.

33 Y. Kawanami, Y. Sonoda, T. Mori and K. Yamamoto, *Org. Lett.*, 2002, **4**, 2825–2827.

34 G. Giordano, R. H. Crabtree, R. M. Heintz, D. Forster and D. E. Morris, *Inorg. Synth.*, 1979, **19**, 218–220.

35 R. Usón, L. A. Oro, J. A. Cabeza, H. E. Bryndza and M. P. Stepro, *Inorg. Synth.*, 1985, **23**, 126–130.

36 (*a*) A. Hamze, O. Provot, J. D. Brion and M. Alami, *J. Organomet. Chem.*, 2008, **693**, 2789–2797; (*b*) A. Hamze, O. Provot, J. D. Brion and M. Alami, *Synthesis*, 2007, 2025–2036; (*c*) S. Nakamura, M. Uchiyama and T. Ohwada, *J. Am. Chem. Soc.*, 2004, **126**, 11146–11147; (*d*) H. Katayama, K. Taniguchi, M. Kobayashi, T. Sagawa, T. Minami and F. Ozawa, *J. Organomet. Chem.*, 2002, **645**, 192–200; (*e*) T. Sudo, N. Asao, V. Gevorgyan and Y. Yamamoto, *J. Org. Chem.*, 1999, **64**, 2494–2499.

37 *SAINT+: Area-Detector Integration Software, version 6.01*, Bruker AXS, Madison, WI, 2001.

38 G. M. Sheldrick, *SADABS program*, University of Göttingen, Göttingen, Germany, 1999.

39 G. M. Sheldrick, *SHELXS 97, Program for the Solution of Crystal Structure*, University of Göttingen, Göttingen, Germany, 1997.

40 G. M. Sheldrick, Crystal structure refinement with SHELXL, *Acta Crystallogr., Sect. C: Struct. Chem.*, 2015, **71**, 3–8.

41 L. J. Farrugia, WinGX and ORTEP for Windows: an Update, *J. Appl. Crystallogr.*, 2012, **45**, 849–854.

42 R. Azpíroz, L. Rubio-Pérez, A. Di Giuseppe, V. Passarelli, F. J. Lahoz, R. Castarlenas, J. J. Pérez-Torrente and L. A. Oro, *ACS Catal.*, 2014, **4**, 4244–4253.

43 M. J. Frisch, G. W. Trucks, H. B. Schlegel, G. E. Scuseria, M. A. Robb, J. R. Cheeseman, G. Scalmani, V. Barone, G. A. Petersson, H. Nakatsuji, X. Li, M. Caricato, A. V. Marenich, J. Bloino, B. G. Janesko, R. Gomperts, B. Mennucci, H. P. Hratchian, J. V. Ortiz, A. F. Izmaylov, J. L. Sonnenberg, D. Williams-Young, F. Ding, F. Lipparini, F. Egidi, J. Goings, B. Peng, A. Petrone, T. Henderson, D. Ranasinghe, V. G. Zakrzewski, J. Gao, N. Rega, G. Zheng, W. Liang, M. Hada, M. Ehara, K. Toyota, R. Fukuda, J. Hasegawa, M. Ishida, T. Nakajima, Y. Honda, O. Kitao, H. Nakai, T. Vreven, K. Throssell, J. A. Montgomery, Jr., J. E. Peralta, F. Ogliaro, M. J. Bearpark, J. J. Heyd, E. N. Brothers, K. N. Kudin, V. N. Staroverov, T. A. Keith, R. Kobayashi, J. Normand, K. Raghavachari, A. P. Rendell, J. C. Burant, S. S. Iyengar, J. Tomasi, M. Cossi, J. M. Millam, M. Klene, C. Adamo, R. Cammi, J. W. Ochterski, R. L. Martin, K. Morokuma, O. Farkas, J. B. Foresman and D. J. Fox, *Gaussian 16, Revision C.01*, Gaussian, Inc., Wallingford, CT, 2019.

44 A. D. Becke, *J. Chem. Phys.*, 1997, **107**, 8554–8560.

45 F. Weigend and R. Ahlrichs, *Phys. Chem. Chem. Phys.*, 2005, **7**, 3297–3305.

46 J. Tomasi, B. Mennucci and R. Cammi, *Chem. Rev.*, 2005, **105**, 2999–3093.